Bone Vol. 31, No. 6
December 2002:675–684

Effects of Transforming Growth Factor-β Deficiency on Bone Development: A Fourier Transform-Infrared Imaging Analysis

E. ATTI,[1,2] S. GOMEZ,[1,3] S. M. WAHL,[4] R. MENDELSOHN,[2] E. PASCHALIS,[1] and A. L. BOSKEY[1]

[1]*Mineralized Tissues Laboratory, Hospital for Special Surgery, New York, NY, USA*
[2]*Department of Chemistry, Rutgers University, Newark, NJ, USA*
[3]*Department of Anatomia Patologica, University of Cadiz, Cadiz, Spain*
[4]*National Institute of Dental and Craniofacial Research, NIH, Bethesda, MD, USA*

Transforming growth factor-beta 1 (TGF-β1) is a cytokine member of the TGF-β superfamily involved in the control of proliferation and differentiation of various cell types. TGF-β1 plays an important role in bone formation and resorption. To determine the effect of TGF-β1 deficiency on bone mineral and matrix, tibias from mice in which TGF-β1 expression had been ablated (TGF-β1 null) were analyzed and compared with background- and age-matched wild-type (WT) control animals by Fourier transform-infrared imaging (FTIRI) and histochemistry. FTIRI allows the characterization of nondemineralized thin tissue sections at the ultrastructural level with a spatial resolution of ∽7 μm. The spectroscopic parameters calculated were: mineral-to-matrix ratio (previously shown to correspond to ash weight); mineral crystallinity (related to the crystallographically determined crystallite size and perfection in the apatite c-axis direction); and collagen maturity (related to the ratio of pyridinoline:deH-DHLNL collagen cross-links). Several fields were selected to represent different stages of bone development within the same specimen from the secondary ossification center to the distal diaphysis. Anatomically equivalent areas were compared as a function of age and genotype. The spectroscopic results were expressed both as color-coded images and as pixel population distributions for each of the three parameters monitored. Based on comparisons of histochemistry and FTIRI, there were distinctive age and genotype variations. At all ages examined, in the TGF-β1 null mice growth plates, alkaline phosphatase (ALP) activity and collagen maturity were reduced, but no effect on mineral content or crystallinity was noted. In the TGF-β1 null mice metaphyses, there was a persistence of trabeculae, but no significant alterations in mineral content or crystallinity. In contrast, mineral content, mineral crystallinity, and collagen maturity were reduced in the secondary ossification center and cortical bone of the TGF-β1 null mice. These results, consistent with a mechanism of impaired bone maturation in the TGF-β1 null mice, may be directly related to TGF-β1 deficiency and indirectly to increased expression of inflammatory cytokines in the TGFβ1 null mice. (Bone 31:675–684; 2002)

Key Words: Transforming growth factor-β (TGF-β); Knockout mouse; Infrared imaging (IR); Mineralization.

Introduction

Transforming growth factor-beta (TGF-β), as reviewed elsewhere,[30,40,53] is an important local regulator of bone metabolism. First isolated from tumor extracts, it was thought to induce a "transformation" between normal and neoplastic cell growth. Since then, TGF-β expression and its role have been examined in essentially every tissue in the body. There are three primary mammalian isoforms (TGF-β1, -β2, and -β3) and distinctive activities for individual members of the TGF-β supergene family and their receptors exist.[9,15–17,27,34,43,48,55] TGFβ1 affects skeletal development and bone homeostasis,[5] playing an important role in the regulation of bone density through its effects on proliferation and differentiation of osteoblasts and on the activity of osteoclasts.[11,20,21,26,56]

TGF-β1 has several effects on cell function that are not directly related to its action on proliferation and differentiation. It influences collagen production and processing by stimulating collagen I peptide synthesis and transcription of collagen I mRNA.[11] Because it has a stimulatory effect on bone regeneration, TGF-β1 has been studied extensively in the field of bone repair,[10] and has been reported to promote fracture healing.[36,44] Because of its involvement in the balance between bone formation and resorption, TGF-β1 has also been studied in the context of osteoporosis.[33,58] The association of variants of the TGF-β1 gene with bone mass indicated a significant association of TGF-β1 polymorphism with osteoporosis.

TGF-β1 also plays an essential role in maintaining normal immune function.[14,15] Approximately 3 weeks after birth, mice having a TGF-β1 null mutation (TGF-β1 knockout) succumb to an inflammatory disease-related organ failure and death.[40] TGF-β1 null mice survive longer if weaning is delayed, providing evidence of a contribution of maternal TGF-β1 to null newborn mice.[35]

D'Souza et al.[19] studied the role of TGF-β1 in tooth mineralization. Dental abnormalities in TGF-β1 null mice were observed and the role of TGF-β1 investigated in odontogenesis at

The first two authors contributed equally to this work.
Address for correspondence and reprints: Dr. Adele L. Boskey, Hospital for Special Surgery, 535 East 70th Street, New York, NY 10021. E-mail: boskeya@hss.edu

8756-3282/02/$22.00
PII S8756-3282(02)00905-5

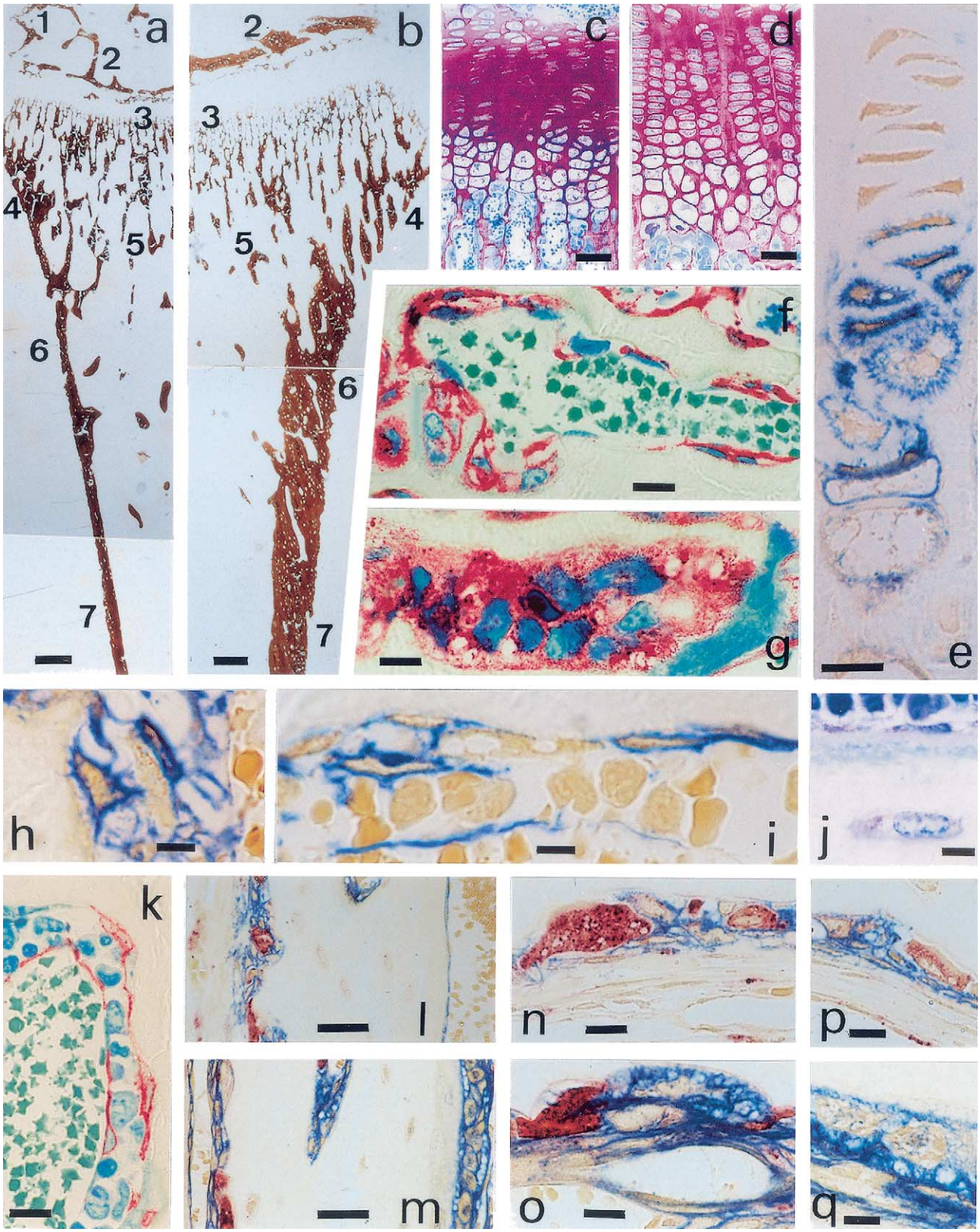

Figure 1. Comparative histology: TGF-β1 null (KO) and WT bones. (a) Panoramic view of KO tibia (25-day-old) stained for mineral. Osteopenia (decreased bone mass) and growth retardation are evident by comparison to WT (b). Labels 1–7 indicate anatomic sites for FTIRI. (1) Calcified articular cartilage in continuity with epiphyseal trabecula; (2) epiphyseal trabeculae; (3) early metaphysis, mainly calcified cartilage cores from epiphyseal growth plate; (4) lateral metaphyseal trabeculae, primary spongiosa; (5) late metaphyseal trabeculae; primary spongiosa; (6) proximal diaphysis

advanced stages by comparison with wild-type mice. A related comparison was used in the present work to investigate the importance of TGF-β1 deficiency for bone mineralization and collagen maturation. The technique of choice was Fourier transform-infrared imaging (FTIRI), a newly developed technique in which an array detector is coupled to an infrared microscope (FTIRM) allowing acquisition of 4096 spectra from 400 μm × 400 μm areas. The advantage of FTIRM and FTIRI over classical FTIR spectroscopy is the detection of the distribution of different chemical species within a spatially inhomogeneous sample.[41,42,50] It was previously shown that both FTIRM and FTIRI analyses of thin tissue sections provide parameters that can be used as a sensitive index of changing mineral properties.[41,42,50] FTIRM and FTIRI of bone can be used to monitor the amount of mineral present,[49] the collagen maturity,[47] and the crystallinity (apatite crystal size and perfection) in bone sections.[22,45,46]

Materials and Methods

TGF-β1 null mice were generated following targeted disruption of the TGF-β1 gene in mouse embryonic stem cells as described elsewhere.[32] Mouse genotype was verified by polymerase chain reaction (PCR) analysis of tail DNA.[28] The mice were weaned between days 14 and 21. Tibias from TGF-β1 null mice (stored before analyses in 90% ethanol) were analyzed and compared with background- and age-matched controls (WT). Animals 7–25 days of age were examined and tibias from three animals were studied for each age and each genotype. Mice aged 7–12 days had no apparent differences relative to controls, and mice typically die after day 26, so this study focused on specimens from 19–25-day-old mice. Tibias from WT and TGF-β1 null mice (KO) were fixed in 70% ethanol, and embedded in glycol methacrylate. Multiple 2 μm sections, obtained using a heavy-duty microtome (Microm HM350, Walldorf, Germany), equipped with a 4 mm blade length diamond knife (Diatome, Switzerland), were used for histology and FTIRI analyses.

Histology

Nondecalcified 2 μm sections were stained with von Kossa, methylene blue, and toluidine blue for routine histology to follow bone growth. The multiple morphologic areas examined included upper epiphysis, epiphyseal plate, metaphysis, and diaphysis. In addition, five tibias from 24- and 25-day-old animals were fixed in 10% phosphate-buffered neutral formalin at 4°C for 6 h and embedded under vacuum with reduced level of catalyst for glycol methacrylate.[25] In this case, 2 μm nondecalcified sections were stained using a simultaneous azo-dye coupling method for alkaline phosphatase (ALP) as an osteoblastic lineage marker, for tartrate-resistant acid phosphatase (TRA-AcP) as an osteoclast marker, or double-stained (ALP/TRA-AcP).[2]

FTIRI

Sections from each of the ethanol-fixed and glycol methacrylate-embedded bones (2 μ thick) were placed on 25 × 2 mm BaF_2 optical disks (windows) and analyzed by means of FTIRI. Seven fields were selected to represent different stages of bone development within the same specimen from epiphysis to distal diaphysis. Anatomically equivalent areas in WT and TGF-β1 null mice were analyzed (**Figure 1**a,b).

Images were collected using a Bio-Rad FTS-6000 Stingray FTIR imaging spectrometer (Bio-Rad, Cambridge, MA), which consists of a step-scan interferometer interfaced to a mercury cadmium telluride (MCT) focal plane array detector imaged to the focal plane of an infrared microscope. Interferograms were simultaneously collected from each element of the 64 × 64 array to provide 4096 spectra at a spectral resolution of 16 cm^{-1}. The array detector enabled spectra from all pixels to be collected simultaneously, yielding an image in which a spectrum could be obtained at each pixel (hyperspectral image). The sample size imaged (400 μm × 400 μm) in a single data collection corresponded to a spatial resolution ranging from 6–10 μm, depending on the wavelength monitored. The instrument software used

(proximal shaft); (7) distal diaphysis (distal shaft). von Kossa stain; bar = 200 μm. (b) Panoramic view of WT tibia (25-day old) stained for mineral. (2)–(7) as in (a). von Kossa; bar = 200 μm. (c) Epiphyseal growth plate of KO (24-day old) is thinner than that of age-matched WT (d). Proliferating and hypertrophic zones are altered. Toluidine blue; bar = 40 μm. (d) Epiphyseal growth plate of WT (24-day-old). Toluidine blue; bar = 40 μm. (e) Detail of growth plate of KO stained for alkaline phosphatase activity (blue) to follow chondrocyte differentiation. Proliferative columns are lacking and hypertrophic chondrocytes are small. Bar = 10 μm. (f) Detail of early metaphysis of KO (24-day-old). Osteogenic cells are located at bone surface but failed to differentiate into osteoblasts. Vessels appear dilated. Alkaline phosphatase staining (red)/ methylene blue; bar = 10 μm. (g) Detail of early metaphysis of WT (24-day-old). In contrast to KO (f), groups of preosteoblastic and osteoblastic cells are present between the two calcified cores. An osteoclast is eroding the tip of both cores. Alkaline phosphatase staining (red)/methylene blue; bar = 10 μm. (h) Detail of early metaphyseal trabeculae in KO tibia (25-day-old). Two osteogenic ells are detected. One is directly located on the bone surface, and the other rests between the existing space limited by the vessels. Note that cytoplasmic prolongation gives them a dendritic habit. These types of cells are unique survivors in the absence of TGF-β1. Alkaline phosphatase staining (blue); bar = 5 μm. (i) Detail of late metaphyseal trabeculae in KO tibia (25-day-old). As in (h), two different osteogenic cells are seen. The first is located on the bone surface and has a running cytoplasmic elongation. The second is in the middle of the marrow cells and may represent an osteoprogenitor reticular cell. No osteoblasts are visible. Alkaline phosphatase staining (blue); bar = 5 μm. (j)Detail of proximal diaphysis at the endosteal side in KO tibia (24-day-old). Note bone surface is quiescent; a lining cell covers a residual osteoid-like layer. Toluidine blue; bar = 5 μm. (k) Epiphyseal trabeculae in KO tibia (24-day-old). Alkaline phosphatase-positive cells are shown on the bone surface. The dilated vessels have reduced the hematopoietic space considerably. Alkaline phosphatase staining (red)/ methylene blue; bar = 10 μm. (l) Panoramic view of proximal diaphysis in KO tibia (24-day-old). Periosteal side is eroding (left). Endosteal side lacks osteoblasts, as contrasted with the WT (m). Alkaline phosphatase (blue)/tartrate-resistant acid phosphatase (red); bar = 20 μm. (m) Panoramic view of proximal diaphysis in WT (24-day-old). Periosteal side is eroding (left). Endosteal side has new bone deposition and an active osteoblast layer. Alkaline phosphatase (blue)/tartrate-resistant acid phosphatase (red); bar = 20 μm. (n) Detail of proximal diaphysis at the periosteal side in KO (24-day-old). Adjacent to a vessel, a recently formed resorption lacuna with an osteoclast shows the presence of periosteal progenitor cells. Preosteoblastic spindle cells are lacking, indicating a retardation of the osteoblastic lineage. Alkaline phosphatase (blue)/tartrate-resistant acid phosphatase (red); bar = 10 μm. (o) Detail of proximal diaphysis at the periosteal side in WT (24-day-old). Adjacent to a vessel, a recent resorption lacuna with an osteoclast is covered by progenitor periosteal cells that proliferate as spindle cells occupying the whole periosteal layer. Alkaline phosphatase (blue)/tartrate-resistant acid phosphatase (red); bar = 10 μm. (p) Detail of the periosteal layer of the distal diaphysis in KO (24-day-old). Osteoclasts persist as well as periosteal progenitor cells. No signs of further proliferation and differentiation of these cells are apparent. Alkaline phosphatase (blue)/tartrate-resistant acid phosphatase (red); bar = 10 μm. (q) Detail of periosteal layer of distal diaphysis in WT (24-day-old). Spindle cells are seen on the outer side, and osteoblast differentiation on the inner. Alkaline phosphatase (blue)/tartrate-resistant acid phosphatase (red); bar = 10 μm.

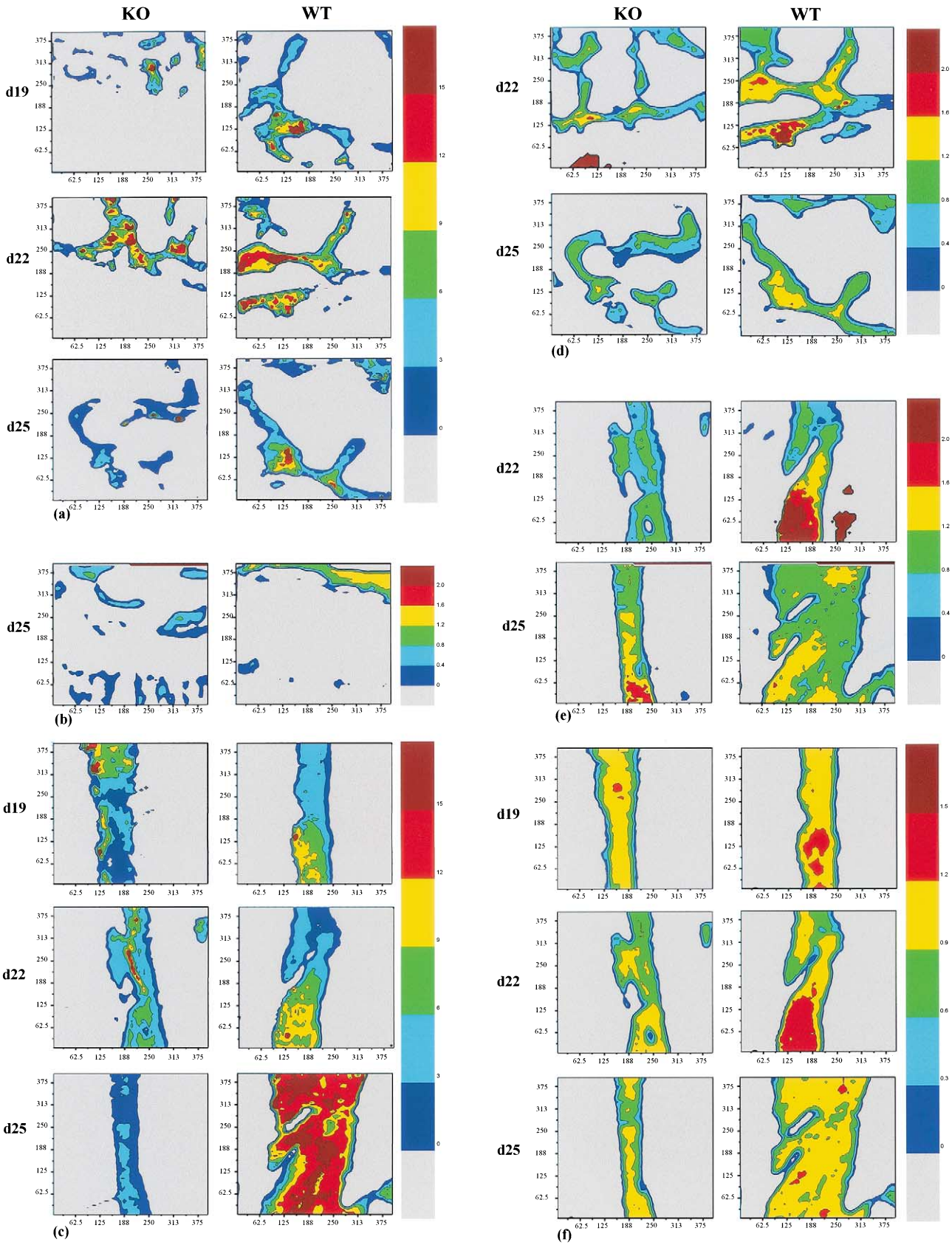

Figure 2. Typical IR images for day 19, day 22, and day 25 WT and KO tibia. (a) Mineral-to- matrix distribution in the secondary ossification

permits straightforward imaging of infrared band areas. For images of peak height ratios and integrated area ratios (see later), software developed in-house was used, based on GRAMS/32 (Galactic Software, Salem, NH), and color-coded images were obtained using MICROCAL ORIGIN (Microcal Origin, Northampton, MA). Histograms were generated with EXCEL 2000 (Microsoft Corp., Redmond, WA), and statistical comparisons performed using INSTAT2 (GraphPad, Inc., Carlsbad, CA).

The spectroscopic parameters calculated were mineral-to-matrix ratio,[49] collagen maturity,[47] and mineral crystallinity.[41,42,45,46,52] The spectroscopic results were expressed both as color-coded images of the three parameters calculated and as pixel population distributions. Mineral-to-matrix ratio was calculated by integrating the area under the peaks at 900–1200 cm^{-1} (phosphate ν_1,ν_3) and ≈1590–1720 cm^{-1} (Amide I) following subtraction of the contribution from glycol methacrylate. The ratio of the integrated phosphate ν_1, ν_3 and Amide I peaks provides a measure of the relative amount of mineral present, a parameter directly related to "ash weight."[49] Crystallinity was expressed by the ratio of the absorbance values at 1030 and 1020 cm^{-1}, respectively. The ratio of the relative areas of these two peaks has previously been shown to provide a sensitive and reproducible index of crystal size and perfection[45,46] and there is a high correlation between peak area and intensity ratio.[41,42] Collagen maturity,[47] expressed in terms of the 1660 and 1690 cm^{-1} intensities, provided an index of the relative ratio of pyridinoline and dehydrodihydroxylysinonorleucine, nonreducible, and reducible collagen cross-links,[31] respectively.

Data Analyses

Baseline correction, integrated peak areas, and intensities (peak heights) were calculated using GRAMS/32 (Galactic). The color-coded images of the three parameters, mineral-to-matrix, 1660/1690, and 1030/1020, were calculated using MICROCAL ORIGIN. The same software was used for the subtraction of the contribution of glycol methacrylate to the mineral and the Amide I absorption. The processed images were expressed as percentage of the pixel population distribution for each of the three parameters monitored. Means and standard deviations were calculated for multiple sections in each animal, and among three different animals for each age using EXCEL (Microsoft). Tests for significant differences between means for the three TGF-β1 null and 3 WT animals at each site and each age were performed using the Bonferroni multiple comparisons test with $p < 0.05$ considered statistically significant (INSTAT, GraphPad).

Results

Our study demonstrated that, after 3 weeks of postnatal development, the TGF-β1-deficient mouse fails to show the pattern of bone mineralization and bone development noted in the age- and background-matched WT animals. This finding was based on histological evaluations, qualitative comparison of infrared images, and quantitative comparisons of pixel histograms derived from the images, and underscores the contribution of TGF-β1 to bone development and homeostasis.

Histology

The first histologically evident differences in bone architecture between TGF-β1 null and WT mice occurred on or after 3 weeks of age. Microscopically, tibias from 22-day-old mice exhibited slightly narrowed growth plates (about 10% that of WT); in early metaphysis, osteoblasts were smaller in size. In the TGF-β1 null epiphyseal trabeculae, osteoblasts were surprisingly lacking, in contrast to the WT epiphyseal trabeculae, which were characterized by active bone remodeling, forming surfaces covered by osteoid borders, and plump osteoblasts. At later timepoints (>24 days), these bone changes were even more dramatic in tibias from TGF-β1 null mice. In these animals, growth retardation was macroscopically evident. Tibias were shorter in length, being 9–11 mm (KO) vs. 12–13 mm (WT). TGFβ1 null tibias had decreased bone mass, apparently at the expense of osteolysis, which was easily detected by comparing von Kossa-stained sections (Figure 1a,b). Growth plate thickness was reduced by about 40%–50% in the TGF-β1 null mice, and chondrocyte alterations such as absence of proliferating columns and absence of full hypertrophic differentiation were striking (Figure 1c–e).

Trabecular bone. Changes were evident in newly formed TGF-β1 null metaphysis, where, in the WT, an area of active bone formation was seen (Figure 1f,g). In the TGF-β1 null mice, capillary vessels appeared dilated, and the osteoblastic population was reduced to the presence of spindle cells, whereas alkaline phosphatase in the preosteoblasts and osteoblasts was completely lacking (Figure 1f). In contrast, numerous osteoblastic clones (osteoprogenitors, preosteoblasts, and osteoblasts) were observed in the WT (Figure 1g). In the rest of the trabecular bone regions (lower metaphyses, epiphyses) the absence of osteoblasts was also noted. However, two types of alkaline phosphatase-positive cells were identified in trabecular bone as survivors of TGF-β1 deprivation. An osteoprogenitor cell, with dendritic cell morphology (Figure 1h,i), was found in the middle of the bone marrow, and a lining cell was found on the mineralized bone surface (Figure 1i). The deficiency of TGF-β1 seemed not to affect osteocytes, because they looked morphologically normal (Figure 1j). A related abnormal architecture was observed at the epiphysis, where the outlined changes of 22-day-old null animals were now easily recognized. Marrow sinusoids were very dilated, and bone marrow cells were enclosed in a reduced space (Figure 1k). The same cavernous aspect was observed in the lower metaphyses and diaphyseal bone marrow (not shown).

Cortical bone. In the endosteum of proximal diaphyses, osteoblasts and osteoid had disappeared in the TGF-β1 null mouse, in contrast to WT (Figure 1l,m). On the periosteal side, the WT proximal diaphyses showed intense modeling activity (Figure 1l,m), characterized by osteoclasts eroding the external cortex, active bone resorption, and proliferating and differentiated osteoblastic cells that produced new bone refilled resorption spaces. This was not the case for TGF-β1 null periosteum (Figure 1l,n). In TGF-β1 null cortex, Howship′s lacunae persisted unfilled, in spite of the finding that, behind the osteoclasts, osteoprogenitor periosteal cells had arrived within the lacuna, but failed to proliferate, as occurs in the WT (Figure 1n,o). As a result of this continued osteoclastic activity, also persistent along

center. (b) Collagen maturity distribution in the growth plate. (c) Mineral-to- matrix distribution in the proximal diaphysis. (d) Collagen maturity in the secondary ossification center. (e) Collagen distribution in the proximal diaphysis. (f) Crystallinity distribution in the same site as in (c). Each area shown represents a 400 μm × 400 μm area. Color scale kept constant for all each parameter.

Bone Vol. 31, No. 6
December 2002:675–684

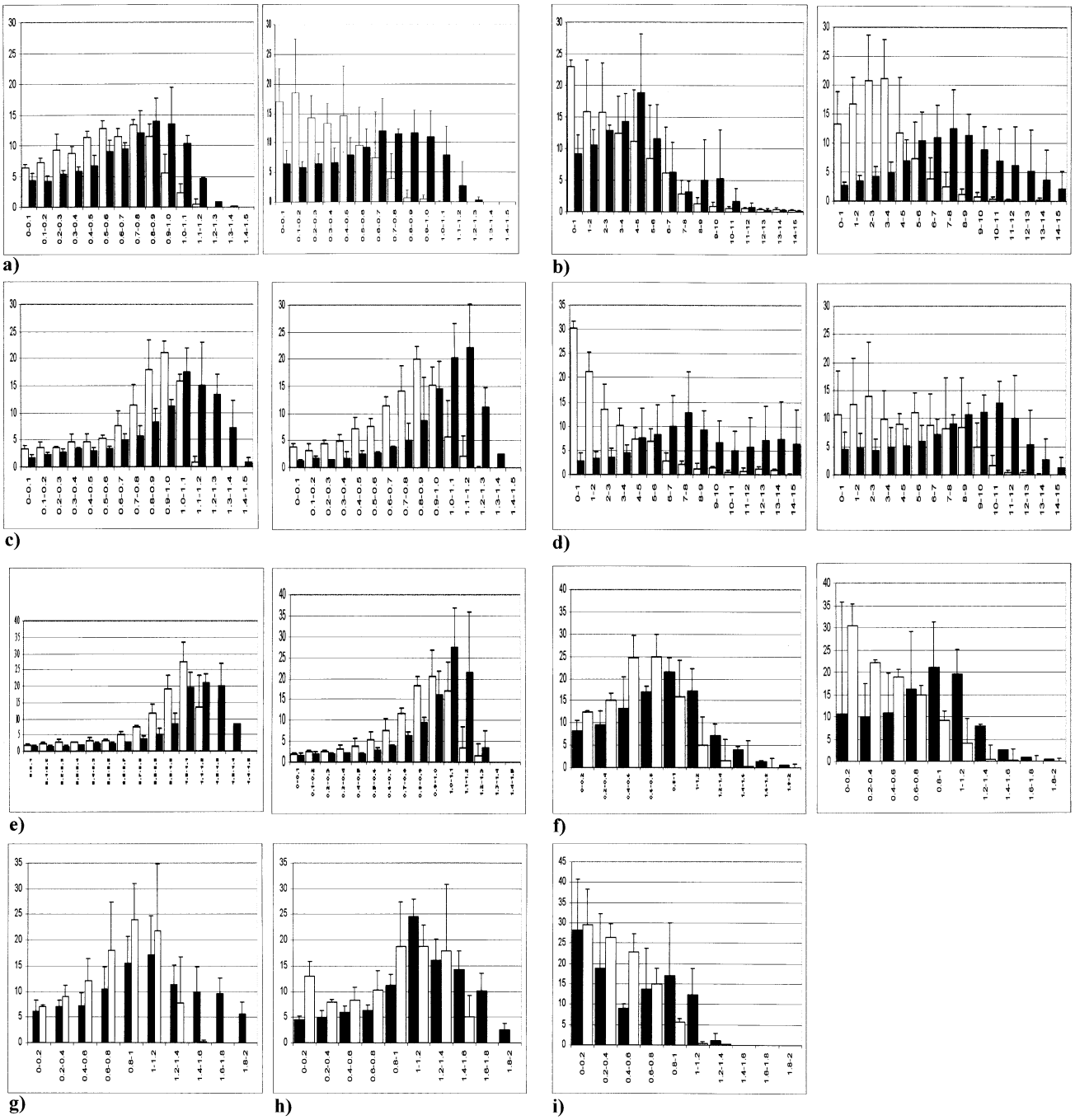

Figure 3. Pixel distribution histograms for all the images from triplicate samples for which individual images are shown in Figure 2. WT, solid bars; KO, open bars. The x axis shows the range of values for each parameter; y axis shows percent of total number of pixels corresponding to the bone image. (a) Crystallinity distribution for the secondary ossification center (22 and 25 days). (b) Mineral-to-matrix distribution for the proximal diaphysis (22 and 25 days). (c) Crystallinity distribution for the proximal diaphysis (22 and 25 days). (d) Mineral-to-matrix distribution for distal diaphysis (22 and 25 days). (e) Crystallinity distribution for the distal diaphysis (22 and 25 days). (f) Collagen maturity distribution for the secondary ossification center (22 and 25 days). (g) Collagen maturity distribution for the proximal diaphysis (22 days). (h) Collagen maturity for the distal diaphysis (22 days). (i) Collagen maturity for the growth plate (25 days).

the distal diaphyses (Figure 1p), cortical thinning was noted, a situation worsened by the absence of forming activity evident in WT (Figure 1q). In TGF-β1 null periosteum neither preosteoblasts nor secretory osteoblasts were identified.

Collectively, these data demonstrate that, at 24 and 25 days postnatally, bone growth and bone formation in the TGF-β1 null mice were practically nonexistent. Trabecular and cortical bone surfaces appeared quiescent and depleted of osteoblastic cells; preexistent osteoblasts were not maintained, having disappeared or transformed into lining cells; and osteoprogenitor cells, although recruited at the proper sites, were unable to sustain any new proliferation.

Table 1. Calculated parameters from FTIRI data of TGF-β1 null (KO) and wild-type (WT) mice

		Day 19	Day 22	Day 25
(A) Mineral: Matrix				
Upper sec. ossif. cen.	KO	3.96 ± 0.98	4.79 ± 1.33	4.19 ± 1.9
	WT	3.06 ± 1.13	3.36 ± 0.95	2.85 ± 1.10
Lower sec. ossif. cen.	KO	3.97 ± 0.31	4.74 ± 1.92	1.96 ± 0.92
	WT	3.88 ± 0.30	4.89 ± 1.63	3.19 ± 0.87
Growth plate	KO	3.77 ± 1.12	3.35 ± 0.10	3.18 ± 1.15
	WT	3.81 ± 0.94	3.40 ± 1.02	4.46 ± 1.55
Newly form. cort.	KO	4.62 ± 0.96	7.76 ± 0.89[a]	5.84 ± 1.07
	WT	4.97 ± 1.22	4.62 ± 0.99	4.96 ± 0.53
Trabecular bone	KO	3.61 ± 0.23[b]	5.00 ± 3.17	3.13 ± 0.62
	WT	6.17 ± 0.37	3.75 ± 1.02	3.60 ± 2.02
Proximal diaphysis	KO	5.37 ± 3.17	3.20 ± 1.36	3.20 ± 0.9[a]
	WT	5.43 ± 1.72	4.42 ± 0.95	8.90 ± 2.3
Distal diaphysis	KO	4.51 ± 1.60	2.52 ± 2.78[a]	4.58 ± 1.86
	WT	6.49 ± 2.75	8.08 ± 2.45	7.75 ± 1.78
(B) Crystallinity				
Upper sec. ossif. cen.	KO	0.40 ± 0.03	0.50 ± 0.02	0.33 ± 0.06
	WT	0.53 ± 0.10	0.58 ± 0.07	0.46 ± 0.08
Lower sec. ossif. cen.	KO	0.31 ± 0.05[b]	0.54 ± 0.04[a]	0.32 ± 0.13[a]
	WT	0.55 ± 0.03	0.69 ± 0.06	0.62 ± 0.07
Growth plate	KO	0.31 ± 0.07	0.34 ± 0.10	0.38 ± 0.07
	WT	0.43 ± 0.08	0.33 ± 0.03	0.52 ± 0.17
Newly form. cort.	KO	0.31 ± 0.04[a]	0.59 ± 0.07	0.53 ± 0.04[a]
	WT	0.47 ± 0.08	0.52 ± 0.05	0.42 ± 0.05
Trabecular bone	KO	0.56 ± 0.10	0.57 ± 0.06	0.46 ± 0.13
	WT	0.47 ± 0.10	0.48 ± 0.06	0.50 ± 0.19
Proximal diaphysis	KO	0.84 ± 0.03[b]	0.74 ± 0.05[b]	0.69 ± 0.06[a]
	WT	0.76 ± 0.16	0.93 ± 0.03	0.93 ± 0.06
Distal diaphysis	KO	0.86 ± 0.08	0.86 ± 0.03[b]	0.80 ± 0.04[a]
	WT	0.96 ± 0.09	1.02 ± 0.03	0.92 ± 0.03
(C) Collagen maturity				
Upper sec. ossif. cen.	KO	0.40 ± 0.12[a]	0.55 ± 0.02[a]	0.46 ± 0.17
	WT	0.61 ± 0.06	0.69 ± 0.08	0.68 ± 0.09
Lower sec. ossif. cen.	KO	0.30 ± 0.10[b]	0.58 ± 0.08[a]	0.42 ± 0.21[a]
	WT	0.67 ± 0.05	0.79 ± 0.10	0.77 ± 0.06
Growth plate	KO	0.23 ± 0.02[a]	0.35 ± 0.18	0.46 ± 0.08[a]
	WT	0.53 ± 0.10	0.30 ± 0.04	0.29 ± 0.05
Newly form. cort.	KO	0.26 ± 0.07[a]	0.59 ± 0.08	0.55 ± 0.08
	WT	0.50 ± 0.06	0.55 ± 0.09	0.46 ± 0.06
Trabecular bone	KO	0.57 ± 0.11	0.63 ± 0.12	0.51 ± 0.11
	WT	0.48 ± 0.11	0.59 ± 0.10	0.55 ± 0.22
Proximal diaphysis	KO	0.90 ± 0.07	0.78 ± 0.11[a]	0.83 ± 0.15
	WT	0.90 ± 0.14	1.03 ± 0.12	1.04 ± 0.17
Distal diaphysis	KO	1.06 ± 0.12	0.83 ± 0.07[a]	0.75 ± 0.17
	WT	1.07 ± 0.10	1.1 ± 0.06	0.94 ± 0.11

[a] $p \leq 0.05$ related to WT at the same age.
[b] $p \leq 0.005$ related to WT at the same age.

FTIRI

Examination of infrared images allowed a qualitative comparison of the spatial variation of mineral content, collagen maturity, and crystallinity. The spectroscopic results expressed both as color-coded images of the three parameters calculated (mineral-to-matrix peak area ratio and 1030/1020 and 1660/1690 intensity ratios) and as pixel population distribution for each of the three parameters monitored are summarized in **Figures 2** and **3**. The pseudo-color of the calculated mineral-to-matrix, collagen maturity, and crystallinity images denote the intensity of the three parameters. The maximum value for all comparable WT and TGFβ1 null mice images was kept constant to facilitate comparison. Statistical evaluation of pixel distributions quantitatively confirmed the qualitative differences in different bone sites examined, without the spatial resolution provided by the images. Visual comparison of images from three replicate bone specimens in the secondary ossification center of 19-day-old animals of the same genotype revealed that the mineral-to-matrix ratios were not different (Figure 2a), although consistently there was less calcified matrix and this matrix indicated reduced mineral content in the TGF-β1 null mice. At 22 days, in contrast to 19 days, the relative mineral content increased in both the WT and the TGFβ1 null mice, but the WT calcified tissues continued to be thicker. The same trends persisted at day 25.

In the proximal diaphysis (Figure 2c) of the 19-day-old WT, there was a lower mineral-to-matrix ratio on the periosteal side, and maximum values on the endosteal side of the bone. Interestingly, the mineral distribution in the TGF-β1 null mice was more uniform. Nonetheless, by day 22, the TGF-β1 null bones tended to be more fragile, and it was difficult to find sections that had not fractured during sectioning. The TGF-β1 null mineral-to-matrix ratio remained low, and comparable to the day 19

Bone Vol. 31, No. 6
December 2002:675–684

cortices, whereas the WT showed an increase in mineral-to-matrix ratio. Mineralization appeared ablated in the TGFβ1 null bones, because, by day 25, the TGF-β1 null did not have a mineral content that differed from day 19 cortices, whereas the mineral-to-matrix ratio was visually increased in the WT.

The crystallinity images corresponding to the mineral-to-matrix distributions in Figure 2c are represented in Figure 2f. The apparent difference in crystallinity implied that mineral crystals, where present, were maturing differently in WT and TGF-β1 null mice. The same pattern was found for the secondary ossification center (images not shown). No significant differences in mineral-to-matrix ratio and crystallinity were observed in the growth plate for all ages.

Figure 2b,d,e illustrates the collagen maturity in these bones. The distribution of mature collagen in the secondary ossification center and proximal diaphysis is shown in Figure 2d,e. Representative patterns are shown for 22- and 25-day-old animals. Significant differences in collagen maturity can be noted upon comparison of WT and TGF-β1 null animals, with the intensity of the collagen maturity parameter higher for WT. Figure 2b shows the distribution of collagen maturity in the growth plate of a 25-day-old animal. The growth plate appears shorter in the TGFβ1 null animal and the collagen appears less mature, comparable to that observed in the 22-day-old animals.

These typical results (which, due to space limitations, are not presented for all sites or ages examined) were confirmed by statistical analysis of the pixel histograms from the combined images. **Table 1** summarizes the results of all ages and areas analyzed for each of the three parameters monitored. First, in the secondary ossification center, there were no significant differences in mineral-to-matrix ratio when age-matched WT and TGF-β1 null were compared (not shown). Crystallinity shifted to lower values in the TGF-β1 null mice (Figure 3a). Analysis of collagen maturity revealed differences between WT and TGF-β1 null animals (shift toward lower values for TGF-β1 null animals) (Figure 3f). Second, trabecular bone did not show differences between age-matched WT and TGF-β1 null animals in the three parameters studied, except for a higher mineral-to-matrix ratio for the WT at day 19. Third, in the proximal diaphysis, a significant shift toward lower values of mineral-to-matrix ratio at 25 days and crystallinity at all ages for the TGF-β1 null mice occurred when contrasted with their age-matched WT (Figure 3b,c). Fourth, the distal diaphysis showed a shift toward lower values of mineral-to-matrix ratio at all ages for TGF-β1 null animals, accompanied by the same trend for crystallinity (Figure 3d,e). In the proximal and distal diaphysis, only the 22-day-old TGF-β1 null mice showed a shift toward lower values of collagen maturity (Figure 3g,h). Finally, analysis of the growth plate showed differences in collagen maturity (Figure 3i), but not in mineral-to-matrix ratio and crystallinity.

Discussion

This study has demonstrated the impact of TGF-β1 deficiency on bone mineralization and collagen maturation. Histochemical data suggest a delayed maturation in the TGF-β1-deficient animals, which was confirmed by quantitative infrared spectroscopy. The technique used, FTIRI, allowed for simultaneous and spatially resolved assessment of the mineral and matrix components of bone. Amount of mineral present, mineral crystallinity, and collagen maturity were evaluated for the first time in TGF-β1 null and WT mice by FTIRI, providing new insights into the effect of deficiency of TGF-β on bone development. The inability to detect significant differences in bone development between TGF-β1 null and WT mice prior to weaning (≤14–19 days) may reflect, in part, the protective effect of maternal transfer of TGF-β.[35] Only upon withdrawal of this source of TGF-β did the true phenotype of the animals become evident. Moreover, products of the emergent inflammatory response[14,15,28,48] may also contribute to bone pathology, although bone is not a typical site of inflammation in these animals. Nonetheless, these changes collectively represent the phenotype of animals deficient in the critical cytokine/growth factor TGF-β1.

TGF-β1 has been shown to have a variety of regulatory actions and represents one of the factors implicated in the regulation of bone turnover. TGF-β1 is a powerful modulator of both bone resorption and bone formation.[5] TGF-β1 influences the mechanisms that regulate skeletal development and skeletal disease, such as osteoporosis. In the TGF-β1-deficient animals, the histochemical features indicated both retarded bone formation and retarded bone remodeling.

The effects of TGF-β1 deficiency on bone maturation identified in this study imply at least two roles for TGF-β1. First, an inductive role for osteogenic cell proliferation (marrow and periosteal), and second an autocrine signal to maintain osteoblasts in a secretory status. In parallel with cessation of maternal TGF-β rescue,[24,35] TGF-β1 null animals, unable to produce endogenous TGF-β, showed growth retardation, as well as chondrocyte and osteoblast aberrancies. It is known from studies combining bromodeoxyuridine incorporation to measure cell proliferation, and assays of alkaline phosphatase activity and bone sialoprotein expression,[2,8] that the osteoblastic lineage includes three important components: osteoprogenitors (stem cells); preosteoblasts (proliferating cells); and osteoblasts (secreting cells). Using alkaline phosphatase (ALP) as an earlier marker for osteoblastic lineage, we demonstrated that, in sites where bone formation is initiated de novo, such as in the primary spongiosa or following bone resorption in Howship′s lacuna, ALP-positive osteoprogenitor cells[3] were present in TGF-β1 null mice, but they failed to proliferate completely and differentiate into new preosteoblasts. An autocrine role was suggested because otherwise secretory osteoblasts were absent, perhaps because of apoptosis or because of transformation to lining ALP-positive cells.[3] However, it was evident in the TGF-β1 null mice that many osteoblasts must die, whereas only a few differentiate into lining cells. In normal bone, the fate of the active osteoblast is either to be buried as an osteocyte, to become a quiescent lining cell, or to die. What regulates this fate is not known. However, TGF-β may influence these pathways because it induces expression of periostin by preosteoblasts,[29] and tenascin-C by osteoblasts.[37]

Our data suggest that secretory osteoblast function is altered in the TGF-β1 null mice and that matrix deposition and mineralization are also dramatically affected. This is particularly evident from 19 to 25 days after birth following weaning. As previously described, the growth plate was also severely altered within both the proliferating compartment and hypertrophic zone, contributing to impaired longitudinal growth.[24] The FTIRI findings suggest a stronger effect of TGF-β1 on collagen maturation rather that on mineralization per se. Only slight differences in the mineral-to-matrix ratio between WT and TGF-β1 null mice were quantitated, even though a trend toward lower values of the mineral-to-matrix and crystallinity parameters was observed. The mineral content appeared to be influenced by the absence of TGF-β1, mainly in the secondary ossification center and cortical bone, wherein mineral apposition appeared slower for the TGF-β1 null animals and bone maturation was impaired. These results are consistent with studies on the effect of TGF-β1 on biomineralization of other tissues such as dentin and enamel.[19]

Disturbances in collagen maturation can also affect mineralization, eventually having an effect on the biomechanical and

functional properties of the tissue. Because TGF-β1 deficiency has been shown in this work to affect collagen maturation, our findings appear consistent with previous studies associating TGF-β1 with osteoporosis, a condition in which collagen maturation is often altered.[47] Collagen I is the predominant extracellular matrix protein component in bone and provides the tissue with tensile strength. TGF-β1 was previously shown to increase collagen production and impact collagen processing.[11] Not only does TGF-β1 stimulate collagen I peptide synthesis and transcription of collagen I mRNA, and enhance the association of secreted collagen,[11] it also influences collagen cross-linking, by affecting the post-translational modification of lysine residues in the newly synthesized collagen α chains.[54] By decreasing the steady-state levels of lysyl hydroxylase mRNA,[54] TGF-β can decrease hydroxylysine residues in bone and consequently influence the properties and biological functions of collagen. Because collagen is important for mineral deposition,[7] disturbances in the post-translational modification of collagen may affect downstream mineralization,[31] although an indirect effect cannot be excluded. If collagen I facilitates the initiation of mineralization and regulates the growth, proliferation, or agglomeration of mineral crystals, then TGF-β1 may be considered to play a crucial role in bone development, addressing its use in a therapeutic approach for osteoporosis.[6,51]

TGF-β1 also influences the osteoblastic production of other bone proteins, such as osteonectin and osteopontin,[4] important for bone mineralization.[7] Thus, the absence of TGF-β1 could lead to alterations in other extracellular matrix components. Consequently, our findings suggest a direct relationship between collagen maturation and TGF-β1 expression, but only imply such a relationship between collagen maturity and mineralization.

TGF-β1 has potent immunomodulatory effects[32,57] with a prevalent suppressive action on proliferating and differentiated inflammatory cells. Although nearly 50% of the homozygous null mice die in utero, those born appear to be normal, and begin to develop inflammatory symptoms within the first week.[38,40] This inflammatory phenotype is exacerbated after weaning, which is likely due in part to the loss of maternal TGF-β1 transferred through the milk.[35] However, immune abnormalities have been detected in day 18 gestation animals,[13] consistent with a requisite role of TGF-β1 in immune development and homeostasis. By 3–4 weeks of age, in the absence of TGF-β1, the TGF-β1 null mice die of a wasting syndrome that resembles an autoimmune syndrome, with a massive infiltration of lymphocytes and macrophages in several genera organs and release of proinflammatory cytokines.[14,15,28] Some of these regulatory molecules, such as interleukin (IL)-1 and IL-6, are potent bone-resorbing factors,[38,39] which may conceivably influence growth retardation and chondrocyte and osteoblast aberrancies. This issue has been investigated previously by Geiser et al.[24] Nonetheless, our data support a pivotal role for TGF-β1 in normal bone development and in crystallinity, collagen deposition, and mineralization. Whether direct or indirect, these fundamental defects in bone biology associated with TGF-β1 deficiency provide insight into possible therapeutic interventional strategies.

Acknowledgments: This study was supported in part by NIH Grants AR03125, AR46121, and DE04141. S.G.'s sabbatical at HSS was granted by the Ministerio de Educacion y Ciencia, and Junta de Andalucía, Spain.

References

1. Bianco, P., Ponzi, A., and Bonucci, E. Basic and "special" stains for plastic sections in bone marrow histopathology, with special reference to May–Grunwald Giemsa and enzyme hystochemistry. Basic Appl Histochem 28:265–279; 1984.
2. Bianco, P., Riminucci, M., Bonucci, E., Termine, J. D., and Gehron Robey, P. Bone sialoprotein (BSP) secretion and osteoblast differentiation: Relationship to bromodeoxyuridine incorporation, alkaline phosphatase, and matrix deposition. J Histochem Cytochem 41:183–191; 1993.
3. Bianco, P., Bradbeer, J. M., Riminucci, M., and Boyde, A. Marrow stromal (Westen–Bainton) cells: Identification, morphometry, confocal imaging and changes in disease. Bone 14:315–320; 1993.
4. Bonewald, L. F. and Mundy, M. D. Role of transforming growth factor-beta in bone remodeling. Clin Orthop 250:261–276; 1990.
5. Bonewald, L. F. Transforming growth factor-β. In: Bilezikian, J. P., Raisz, L. G., & Rodan, G. A., eds. Principles of Bone Biology. San Diego, CA: Academic; 647–659; 1996.
6. Boonen, S., Broos, P., Dequeker, J., and Bouillon, R. The prevention of treatment of age-related osteoporosis in the elderly by systemic recombinant growth factor therapy (rhIGF-I or rhTGFβ): A perspective. J Intern Med 242:285–290; 1997.
7. Boskey, A. L. Matrix protein and mineralization: An overview. Connect Tissue Res 35:357–363; 1996.
8. Bruder, S. P., Horowitz, M. C., Mosca, J. D., and Haynesworth, S. E. Monoclonal antibodies reactive with human osteogenic cell surface antigens. Bone 21:225–235; 1997.
9. Cam, Y., Neumann, M. R., and Ruch, J. V. Immunolocalization of TGF-β1 and EGF-receptor epitopes in mouse incisors and molars. Demonstration of *in vitro* production of transforming activity. Arch Oral Biol 35:813–822; 1990.
10. Carrington, J. L., Roberts, A. B., Flanders, K. C., Roche, N. S., and Reddi, A. H. Accumulation, localization, and compartmentation of transforming growth factor beta during endochondral bone development. J Cell Biol 107: 1969–1975; 1988.
11. Centrella, M., Casinghino, S., Ignotz, R., and McCarthy, T. L. Multiple effects by transforming growth factor-β on type I collagen levels in osteoblast-enriched cultures from fetal rat bone. Endocrinology 131:2863–2872; 1992.
12. Centrella, M., Horowitz, M. C., Wozney, J. M., and McCarthy, T. L. Transforming growth factor-β gene family members and bone. Endocrine Rev 15:27–39; 1994.
13. Chen, W., Jin, W., Tian, H., Sicurello, P., Frank, M., Orenstein, J. M., and Wahl, S. M. Requirement for transforming growth factor beta1 in controlling T cell apoptosis. J Exp Med 194:439–453; 2001.
14. Chen, W. and Wahl, S. M. Manipulation of TGF-beta to control autoimmune and chronic inflammatory disease. Microbes Infect 1:1367–380; 1999.
15. Christ, M., McCartney-Francis, N. L., Kulkarni, A. B., Ward, J. M., Mizel, D. E., Mackall, C. L., Gress, R. E., Hines, K. L., Tian, H., and Karlsson, S. Immune dysregulation in TGF-β1-deficient mice. J Immunol 153:1936–1946; 1994.
16. D'Souza, R. N., Happonen, R. P., Ritter, N. M., and Butler, W. T. Temporal and spatial patterns of transforming growth factor-beta1 expression in developing rat molars. Arch Oral Biol 35:957–965; 1990.
17. D'Souza, R. N., Happonen, R. P., Flanders, K. C., and Butler, W. T. Histochemical localization of transforming growth factor-β1 in developing rat molars using antibodies to different epitopes. J Biol Buccale 18:299–306; 1990.
18. D'Souza, R. N., Flanders, K. C., and Butler, W. T. Colocalization of TGF-beta1 and extracellular matrix proteins during rat tooth development. Proc Fin Dent Soc 88(Suppl. 1):419–426; 1992.
19. D'Souza, R. N., Cavender, A., Sood, R., Tarnuzzer, R., Dickinson, D. P., Roberts, A., and Letterio, J. Dental abnormalities in mice lacking a functional transforming growth factor-β1 (TGF-β1) gene indicate a role for TGF-β1 in biomineralization. Int J Oral Biol 23:119–131; 1998.
20. Erlebacher, A., Filvaroff, E. H., Ye, J. Q., and Derynck, R. Osteoblastic responses to TGF-β during bone remodeling. Mol Biol Cell 9:1903–1918; 1998.
21. Erlebacher, A. and Derynck, R. Increased expression of TGF-β2 in osteoblasts results in an osteoporosis-like phenotype. J Cell Biol 132:195–210; 1996.
22. Gadaleta, S. J., Paschalis, E. P., Betts, F., Mendelsohn, R., and Boskey, A. L. Fourier transform infrared spectroscopy of the solution-mediated conversion of amorphous calcium phosphate to hydroxyapatite: New correlations between X-ray diffraction and infrared data. Calcif Tissue Int 58:9–16; 1996.
23. Gadaleta, S. J., Boskey, A. L., Paschalis, E., Carlson, C., Menschik, F., Baldini, T., Peterson, M., and Rimnac, C. M. A physical, chemical, and mechanical study of lumbar vertebrae from normal, ovariectomized, and nandrolone decanoate-treated cynomolgus monkeys (*Macaca fascicularis*). Bone 27:541–550; 2000.

24. Geiser, A. G., Zeng, Q. Q., Sato, M., Helvering, L. M., Hirano, T., and Turner, C. H. Decreased bone mass and bone elasticity in mice lacking the transforming growth factor-β1 gene. Bone 23:87–93; 1998.
25. Gomez, S. and Boyde, A. Correlated alkaline phosphatase histochemistry and quantitative backscattered electron imaging in the study of rat incisor ameloblasts and enamel mineralization. Microsc Res Techn 29:29–36; 1994.
26. Hauschka, P. V., Mavrakos, A. E., Iafrati, M. D., Doleman, S. E., and Klagsbrun, M. Growth factors in bone matrix. Isolation of multiple types by affinity chromatography on heparin-sepharose. J Biol Chem 261:12665–12674; 1986.
27. Heikinheimo, K., Happonem, R. P., Miettinen, P. J., and Ritvos, O. Transforming growth factor beta 2 in epithelial differentiation of developing teeth and odontogenic tumors. J Clin Invest 91:1019–1027; 1993.
28. Hines, K. L., Kulkarni, A. B., McCarthy, J. B., Tian, H., Ward, J. M., Christ, M., McCartney-Francis, N. L., Furcht, L. T., Karlsson, S., and Wahl, S. M. Synthetic fibronectin peptides interrupt inflammatory cell infiltration in transforming growth factor β1 knockout mice. Proc Natl Acad Sci USA 91:5187–5191; 1994.
29. Horiuchi, K., Amizuka, N., Takeshita, S., Takamatsu, H., Katsuura, M., Ozawa, H., Toyama, Y., Bonewald, L. F., and Kudo, A. Identification and characterization of a novel protein, periostin, with restricted expression to periosteum and periodontal ligament and increased expression by transforming growth factor β. J Bone Miner Res 14:1239–1249; 1999.
30. Kinsley, D. M. The TGF-beta superfamily: New members, new receptors, and new genetic test of function in different organisms. Gene Devel 8:133–146; 1994.
31. Knott, L. and Bailey, A. J. Collagen cross-links in mineralized tissues: A review of their chemistry, function, and clinical relevance. Bone 22:181–187; 1998.
32. Kulkarni, A. B., Huh, C-G, Becker, D., Geiser, A., Lyght, M., Flanders, K. C., Roberts, A. B., Sporn, M. B., Ward, J. M., and Karlsson, S. Transforming growth factor β1 null mutation in mice causes excessive inflammatory response and early death. Proc Natl Acad Sci USA 90:770–774; 1993.
33. Langdahl, B. L., Knudsen, J. Y., Jensen, H. K., Gregersen, N., and Eriksen, E. F. A sequence variation: 713-8delC in transforming growth factor-β1 gene has higher prevalence in osteoporotic women that in normal women and is associated with very low bone mass in osteoporotic and normal woman. Bone 20:289–294; 1997.
34. Lehnert, S. A. and Akhurst, R. J. Embryionic expression pattern of TGF beta type-1 RNA suggests both paracrine and autocrine mechanisms of action. Development 104:263–273; 1988.
35. Letterio, J. J., Geiser, A. G., Kulkarni, A. B., Roche, N. S., Sporn, M. B., and Roberts, A. B. Maternal rescue of transforming growth factor-beta 1 null mice. Science 24 264:1936–1994; 1938.
36. Lind, M., Schumacker, B., Soballe, K., Keller, J., Melsen, F., and Bunger, C. Transforming growth factor-beta enhances fracture healing in rabbit tibiae. Acta Orthop Scand 64:553–556; 1993.
37. Mackie, E. J., Abraham, L. A., Taylor, S. L., Tucker, R. P., and Murphy, L. I. Regulation of tenascin-C expression in bone cells by transforming growth factor-β. Bone 22:301–307; 1998.
38. Manolagas, S. C. and Jilka, R. Bone marrow, cytokines, and bone remodeling: Emerging insights into the pathophysiology of osteoporosis. N Engl J Med 232:305–311; 1995.
39. Manolagas, S. C. Role of cytokines in bone resorption. Bone 17(Suppl.):63S–67S; 1995.
40. McCartney-Francis, N. L., Frazier-Jessen, M., and Wahl, S. M. TGF-beta: A balancing act. Int Rev Immunol 16:553–580; 1998.
41. Mendelsohn, R., Paschalis, E. P., and Boskey, A. L. Infrared spectroscopy, microscopy and microscopic imaging of mineralized tissues: Spectra–structure correlations from human iliac crest biopsies. J Biomed Optics 4:14–21; 1999.
42. Mendelsohn, R., Paschalis, E. P., Sherman, P. J., and Boskey, A. L. IR Microscopic imaging of pathological states and fracture healing of bone. Appl Spectrosc 54:1183–1191; 2000.
43. Millan, F. A., Denhez, F., Kondaiah, P., and Akhrust, R. J. Embryonic gene expression patterns of TGF beta 1, beta 2 and beta 3 suggest different developmental function *in vivo*. Development 111:131–143; 1991.
44. Nielsen, H. M., Andreassen, T. T., Ledet, T., and Oxlund, H. Local injection of TGF-beta increases the strength of tibial fractures in the rat. Acta Orthop Scand 65:37–41; 1994.
45. Paschalis, E. P., DiCarlo, E., Betts, F., Sherman, P., Mandelsohn, R., and Boskey, A. L. FTIR microspectropic analysis of human osteonal bone. Calcif Tissue Int 59:480–487; 1996.
46. Paschalis, E. P., Betts, F., DiCarlo, E., Mendelsohn, R., and Boskey, A. L. FTIR microspestroscopic analysis of normal human cortical and trabecular bone. Calcif Tissue Int 61:480–486; 1997.
47. Paschalis, E. P., Verdelis, K., Doty, S. B., Boskey, A. L., Mendelsohn, R., and Yamauchi, M. Spectroscopic characterization of collagen cross-links in bone. J Bone Miner Res 16:1821–1828; 2001.
48. Pelton, R. W., Saxena, B., Jones, M., Moses, H. L., and Gold, L. I. Immunohistochemical localization of TGF beta 1, TGF beta 2, and TGF beta 3 in the mouse embryo: Expression patterns suggest multiple roles during embryonic development. J Cell Biol 115:1091–1105; 1991.
49. Pienkowski, D., Doers, T. M., Monier-Faugere, M. C., Geng, Z., Camacho, N. P., and Boskey, A. L. Calcitonin alters bone quality in beagle dogs. J Bone Miner Res 12:1936–1943; 1997.
50. Pleshko, N. L., Boskey, A. L., and Mendelsohn, R. Novel infrared spectroscopic method for the determination of crystallinity of hydroxyapatite minerals. Biophys J 60:786–793; 1991.
51. Prestwood, K. M., Pilbeam, C. C., and Raisz, L. G. Treatment of osteoporosis. Annu Rev Med 46:249–256; 1995.
52. Rey, C., Shimizu, M., Collins, B., and Glimcher, M. J. Resolution-enhanced Fourier transform infrared spectroscopy study of the environment of phosphate ion in the early deposits of a solid phase calcium phosphate in bone and enamel and their evolution with age: 2. Investigation in the ν_3 PO_4 domain. Calcif Tissue Int 49:383–388; 1991.
53. Roberts, A. B. and Sporn, M. B. Transforming growth factor-β. In: Clark, R. A. F., ed. The Molecular and Cellular Biology of Wound Repair. New York: Plenum; 275–308; 1995.
54. Seitzer, U., Bätge, B., Acil, Y., and Müller, P. K. Transforming growth factor b1 influences lysil hydroxylation of collagen I and reduces steady-state levels of lysyl hydroxylase mRNA in human osteoblasts-like cells. Eur J Clin Invest 25:959–966; 1995.
55. Serra, R., Johnson, M., Filvaroff, E. H., La Borde, J., Sheehan, D. M., Derynck, R., and Moses, H. L. Expression of truncated, kinase-defective TGF-β type II receptor in mouse skeletal tissue promotes terminal chondrocyte differentiation and osteoarthritis. J Cell Biol 139:541–552; 1997.
56. Vaahtokary, A., Vainio, S., and Thesleff, I. Associations between transforming growth factor beta 1 RNA expression and epithelial–mesenchymal interactions during tooth morphogenesis. Development 113:985–994; 1991.
57. Wahl, S. M., McCartney-Francis, N., and Mergenhagen, S. E. Inflammatory and immunomodulatory roles of TGF-β. Immunol Today 10:258–261; 1989.
58. Yamada, Y., Miyauchi, A., Goto, J., Takagi, Y., Okuizumi, H., Kanematsu, M., Hase, M., Takai, H., Harada, A., and Ikeda, K. Association of a polymorphism of the transforming growth factor beta1 gene with genetic susceptibility to osteoporosis in postmenopausal women. J Bone Miner Res 13:1569–1576; 1998.

Date Received: December 21, 2001
Date Revised: June 19, 2002
Date Accepted: July 31, 2002